Journal of Materials Science and Chemical Engineering, 2017, 5, 129-141
http://www.scirp.org/journal/msce
ISSN Online: 2327-6053
ISSN Print: 2327-6045

Enhanced Visible-Light-Sensitive Two-Step Overall Water-Splitting Based on Band Structure Controls of Titanium Dioxide and Strontium Titanate

Satoshi Tanigawa[1], Toshihiro Takashima[1,2], Hiroshi Irie[1,2*]

[1]Special Doctoral Program for Green Energy Conversion Science and Technology, Interdisciplinary Graduate School of Medicine and Engineering, University of Yamanashi, Yamanashi, Japan
[2]Clean Energy Research Center, University of Yamanashi, Yamanashi, Japan
Email: *hirie@yamanashi.ac.jp

How to cite this paper: Tanigawa, S., Takashima, T. and Irie, H. (2017) Enhanced Visible-Light-Sensitive Two-Step Overall Water-Splitting Based on Band Structure Controls of Titanium Dioxide and Strontium Titanate. *Journal of Materials Science and Chemical Engineering*, **5**, 129-141.
http://dx.doi.org/10.4236/msce.2017.51017

Received: December 22, 2016
Accepted: January 20, 2017
Published: January 23, 2017

Abstract

Visible light-induced two-step overall water-splitting was achieved by combining two types of photocatalysts, which were prepared by introducing foreign elements into rutile titanium dioxide (TiO_2) and strontium titanate ($SrTiO_3$) with a controlled electronic band structure. Rutile TiO_2 and $SrTiO_3$ were doped with chromium and tantalum (Cr,Ta-TiO_2) and with rhodium (Rh-$SrTiO_3$), respectively, to introduce visible-light sensitivity. Under irradiation with only visible light from a 420-nm LED lamp, the simultaneous liberation of hydrogen and oxygen with a molar ratio of ~2:1 was achieved with these two types of photocatalysts in the presence of iodate ion/iodide ion as a redox mediator.

Keywords

Titanium Dioxide, Strontium Titanate, Visible Light, Overall Water-Splitting, Two-Step Excitation

1. Introduction

Various photocatalytic materials have been evaluated for water splitting activity because the generated hydrogen (H_2) represents a clean and renewable fuel source [1] [2] [3]. Among examined materials, titanium dioxide (TiO_2) with which Fujishima and Honda first demonstrated photoinduced water-splitting [1] and strontium titanate ($SrTiO_3$) [4], are the most promising photocatalysts due to their abundance, nontoxicity, thermal stability and high resistance against

photo-corrosion. Despite these advantageous properties, both TiO_2 and $SrTiO_3$ are only sensitive to ultraviolet (UV) light and therefore requires modification for the utilization of visible light. To this end, numerous studies have examined the effects of doping foreign elements into TiO_2 and $SrTiO_3$ on visible-light induced water-splitting [5] [6] [7] [8]. Although a sacrificial agent is needed, the doped TiO_2 and $SrTiO_3$ are able to generate either H_2 or oxygen (O_2) following irradiation with visible light (half reaction of water-splitting).

Combined systems consisting of two specific photocatalysts for H_2 and O_2 production (H_2-photocatalyst and O_2-photocatalyst, respectively) and a suitable redox mediator can function as visible-light sensitive photocatalysts for overall water-splitting (termed two-step overall water-splitting or Z-scheme overall water-splitting) [9]-[18]. The well-known combination is platinum (Pt)-deposited chromium (Cr) and tantalum (Ta)-codoped $SrTiO_3$ or ruthenium (Ru)-deposited rhodium (Rh)-doped $SrTiO_3$ as the H_2-photocatalyst, and Pt-deposited tungsten trioxide (WO_3) or bismuth vanadate ($BiVO_4$) as the O_2-photocatalyst [10] [11]. The Z-scheme systems require the suitable redox mediator, such as iodate (IO_3^-)/iodide (I^-) or ferric (Fe^{3+})/ferrous (Fe^{2+}) ions. Recently, solid-state Z-scheme systems that function in the absence of a redox mediator have been reported [13]-[18].

Our group have successfully synthesized a combined system consisting of only one mother material, TiO_2-based photocatalysts (Pt-deposited anatase $Ti_{0.96}Cr_{0.02}Ta_{0.02}O_2$ ($Pt/Ti_{0.96}Cr_{0.02}Ta_{0.02}O_2$) and Pt-deposited rutile $Ti_{0.982}Cr_{0.009}Ta_{0.009}O_2$ ($Pt/Ti_{0.982}Cr_{0.009}Ta_{0.009}O_2$) as the H_2- and O_2-photocatalyst, respectively) and $SrTiO_3$-based photocatalysts (Ru-deposited $Sr(Ti_{0.99}Rh_{0.01})O_3$ and Ru-deposited $(Sr_{0.99}Na_{0.01})(Ti_{0.99}V_{0.01})O_3$, as the H_2- and O_2-photocatalyst, respectively) [19] [20]. Based on the activities of the systems, it was conceivable that visible-light-sensitive two-step overall water-splitting system could be improved by utilizing the $SrTiO_3$- and TiO_2-based materials as H_2- and O_2-photocatalysts, respectively. The construction of such a system may be advantageous because they have properties, such as nontoxicity, stability, and natural abundance, which are expected to facilitate their use in industrial and practical applications by contrast with utilization of WO_3 or $BiVO_4$.

In the present study, we combined Cr- and Ta-codoped TiO_2 and Rh-doped $SrTiO_3$, and achieved the H_2- and O_2-evolution rates derived from two-step overall watersplitting ~100 times larger irradiated with 420-nm visible-light.

2. Experimental Section

2.1. Preparations of TiO_2-Based and $SrTiO_3$-Based Photocatalysts

Cr- and Ta-codoped rutile TiO_2 ($Ti_{0.986}Cr_{0.007}Ta_{0.007}O_2$, Cr,Ta-$TiO_2$) as an O_2-evolution photocatalyst was prepared by a hydrothermal synthesis method using commercial $Ti(SO_4)_2$ (24.0% purity, 3.97×10^{-2} mol; Kanto Kagaku), $CrCl_3 \cdot 6H_2O$ (1.40×10^{-4} mol; Kanto Kagaku), and $TaCl_5$ (1.40×10^{-4} mol; Kanto Kagaku) as starting materials. The starting materials for the form of Cr,Ta-TiO_2 were mixed and stirred in distilled water for 30 min using a magnetic stirrer. The solutions

were treated hydrothermally in an autoclave at 140˚C for 12 h, and the resulting mixtures were washed with sufficient distilled water, collected by centrifugation, and dried at 80˚C overnight. The dried mixtures were calcined at 900˚C for 24 h, and were then thoroughly ground using a mortar and pestle. As a reference, non-doped rutile (TiO_2) was prepared under identical conditions using only $Ti(SO_4)_2$.

Rh-doped $SrTiO_3$ ($Sr(Ti_{0.99}Rh_{0.01})O_3$, Rh-$SrTiO_3$) was synthesized using a conventional solid-state reaction. Commercial $SrCO_3$ (Kanto Kagaku, purity 99.9%), TiO_2 (High Purity Chemicals, purity 99.99%), and Rh_2O_3 (Kanto Kagaku, purity 99.9%) powders were used as the starting materials. Stoichiometric amounts of the starting materials for Rh-$SrTiO_3$ were wet-ball-milled (200 rpm) for 20 h using zirconium dioxide (ZrO_2) balls as the milling medium in polyethylene bottles. The resulting mixture was calcined at 1000˚C for 10 h and then thoroughly ground to obtain Rh-$SrTiO_3$ powder. As a reference, non-doped $SrTiO_3$ was prepared under identical conditions using only $SrCO_3$ and TiO_2.

The deposition of either Pt or Ru co-catalyst onto the synthesized Cr,Ta-TiO_2 or Ru-$SrTiO_3$ photocatalysts, respectively, was performed by a photo-deposition method. Briefly, 0.5 g of either Cr,Ta-TiO_2 or Ru-$SrTiO_3$ powder was first dispersed in 100 mL methanol solution (20 vol%) as a hole scavenger. The amount of $H_2PtCl_6{\cdot}6H_2O$ (98.5% purity; Kanto Kagaku) as the source of Pt needed to give a weight fraction of Pt relative to Cr,Ta-TiO_2 of 1×10^{-3} was weighted. Ruthenium chloride ($RuCl_3{\cdot}nH_2O$, n was assumed to be 3), which served as the source of Ru, was weighed to give a weight fraction of Ru relative to Rh-$SrTiO_3$ of 7×10^{-3}. Weighed $H_2PtCl_6{\cdot}6H_2O$ or $RuCl_3{\cdot}nH_2O$ was added to each aqueous sample suspension, which was then sufficiently deaerated using liquid nitrogen (N_2). While deaerating the suspensions, a xenon (Xe) lamp (LA-251 Xe; Hayashi Tokei) equipped with an optical filter (Y-44, Hoya) was employed for light irradiation of the suspension for 4 h. The suspension was then centrifuged, washed with distilled water, and the resulting residues were dried at 80˚C overnight. The residues were ground into a fine powder using an agate mortar to obtain the Pt-deposited Cr,Ta-TiO_2 (Pt/Cr,Ta-TiO_2) and Ru-deposited Rh-$SrTiO_3$ (Ru/Rh-$SrTiO_3$) photocatalyst powders.

2.2. Characterizations

The crystal structures of the prepared powders were examined by X-ray diffraction (XRD) using a PW-1700 system (Panalytical). Brunauer-Emmett-Teller (BET) surface areas were determined using a nitrogen adsorption apparatus (Micromeritics, TriStar 3000; Shimadzu). The valency of the constituent elements was measured by X-ray photoelectron spectroscopy (XPS; Axis-Ultra, Shimadzu). UV-visible absorption spectra were obtained by the diffuse reflection method using a V-650 (JASCO) spectrometer. Quantitative analyses were performed by X-ray fluorescence (XRF) using a ZSXP PrimusII system (Rigaku). A scanning transmission electron microscope (STEM, Tecnai Osiris, FEI) were used to observe the morphology of the prepared photocatalysts.

2.3. Photocatalytic Water-Splitting Tests

Two types of photocatalytic water-splitting tests (half reactions of water-splitting and two-step overall water-splitting) were performed in a gas-closed-circulation system, which was filled with argon gas (50 kPa) after deaeration. The amounts of evolved H_2 and O_2 were monitored using an online gas chromatograph (GC-8A; Shimadzu). Each time we performed the water-splitting experiments, a different amount of N_2 was detected. We repeatedly deaerated this system to a final pressure of 2.5 Pa and then introduced argon gas into the system in the same way. For these reasons, we considered that the detection of N_2 originated from the intruded air from outside, and the effect of residual O_2 (and N_2) in water was possibly excluded [19] [20] [21]. Thus, if N_2 was detected, the O_2 amount was calculated using the following equation: O_2 = obs. O_2 – (obs. N_2/0.78) × 0.21.

H_2 and O_2 evolution derived from the half reaction of water-splitting was monitored in the presence of Ru/Rh-$SrTiO_3$ or Pt/Cr,Ta-TiO_2 (60 mg each) with the aid of iodide ion (I^-) (sodium iodide (NaI), 99.5% purity, 0.01 mol/L Kanto Kagaku) or iodate ion (IO_3^-) (sodium iodate ($NaIO_3$), 99.5%purity, 0.01 mol/L; Kanto Kagaku), respectively, as a sacrificial agent. The examinations were conducted in 10 mL of solution, without adjusting the pH, with constant stirring using a magnetic stirrer and under irradiation with visible light generated from a light-emitting diode (LED) lamp with a wavelength of 420 nm (420 nm-LED, LEDH60-420, Hamamatsu Photonics). Two-step overall water-splitting experiments were conducted by adding the sample powders (Ru/Rh-$SrTiO_3$: 10 mg, Pt/Cr,Ta-TiO_2: 50 mg) to 10 mL IO_3^- solution as a starting redox mediator without I^-. The suspension was constantly stirred using a magnetic stirrer and the pH was not adjusted. The 420 nm-LED light was used for light irradiation.

3. Results and Discussion

3.1. Characterization of the Prepared Photocatalysts

Elemental analysis by XRF indicated that the molar ratio of Ti:Cr:Ta in Pt/Cr,Ta-TiO_2 was 0.994:0.002:0.004. Notably, this molar ratio was not consistent with the starting ratios used in the preparation of the photocatalyst. This discrepancy was attributed to differences in the solubility of Ti, Cr and Ta in aqueous solution under hydrothermal conditions. The analysis also indicated that the molar fraction of Pt relative to Cr,Ta-TiO_2 was 1×10^{-4}. The analysis indicated that the molar ratios of Sr:Ti:Rh in Rh/Rh-$SrTiO_3$ was 0.493:0.493:0.014 nearly equal to the starting fractions used in the preparation. The Ru amount relative to Rh-$SrTiO_3$ was observed to be 1×10^{-2}.

Cr,Ta-TiO_2 was confirmed to have a single phase of rutile TiO_2, in the obtained XRD spectrum (**Figure 1(a)**). In addition, the XRD peaks of Cr,Ta-TiO_2 were shifted to a lower 2θ angle compared to non-doped TiO_2 (**Figure 1(b)**). These results are reasonable when one considers that the effective ionic radii of Ti^{4+}, Cr^{3+}, and Ta^{5+} (six-coordination) are 0.0605, 0.0615, and 0.064 nm,

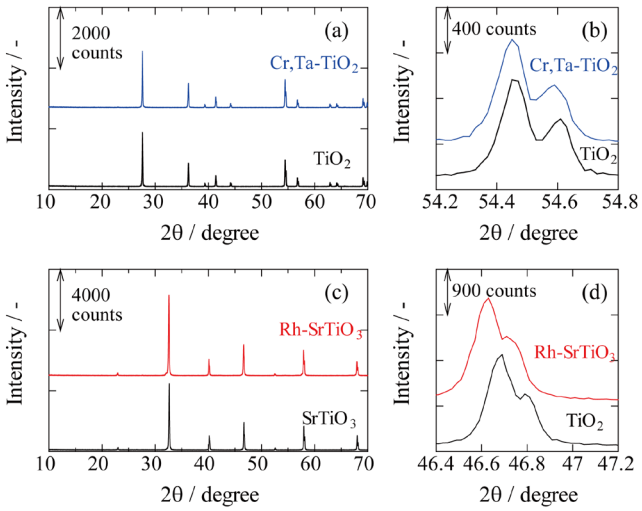

Figure 1. XRD patterns of prepared TiO_2 and Cr,Ta-TiO_2 powders (a), and $SrTiO_3$ and Rh-$SrTiO_3$ (c). (b) and (d) are enlargements of (a) and (c), respectively.

respectively [22]. Thus, in the rutile form of the TiO_2 photocatalyst, Cr and Ta ions were incorporated at Ti sites. The XRD pattern of the synthesized Rh-$SrTiO_3$ powder indicated the photocatalyst formed a cubic crystal structure with a perovskite crystalline phase (**Figure 1(c)**). In **Figure 1(d)**, the peak of Rh-$SrTiO_3$ shifted to a lower 2θ angle compared to non-doped $SrTiO_3$. According to Konda *et al.* [23], two different species of Rh (Rh^{3+} (0.0665 nm, the effective ionic radius) and a Rh species with a higher oxidation state than Rh^{3+}, such as Rh^{4+} (0.0615 nm, the same)) replaced Ti sites as dopants. Thus, we considered that Rh ions were incorporated at Ti sites in $SrTiO_3$.

XPS spectra were recorded to confirm the valency of constituent ions in Cr,Ta-TiO_2 and Rh-$SrTiO_3$. **Figures 2(a)-2(d)** show the spectra for the Ti 2p, Cr 2p, Ta 4f, and O1s orbitals, respectively, of the prepared TiO_2, Cr,Ta-TiO_2, and commercially available TiO_2 (99% purity, Kanto Kagaku) after calibration with the C 1s peak, derived from a conductive carbon-tape that had a binding energy of 284.5 eV. The spectra of Ti 2p of the prepared TiO_2 and Cr,Ta-TiO_2 were quite similar without any shoulder or peak at lower binding energy side (**Figure 2(a)**). Thus, the valency of Ti was 4+ in the prepared TiO_2 and Cr,Ta-TiO_2 [24] [25]. In contrast, the commercial TiO_2 had the peaks at lower binding energy side, indicating that it includes Ti^{3+} [24]. The Cr 2p peaks derived from Cr^{3+} (Cr $2p_{3/2}$ at 576.9 eV and $Cr2p_{1/2}$ at 587.0 eV [24]) and Ta 4f peaks from Ta^{5+} (Ta $4f_{7/2}$ at 26 eV and Ta $4f_{5/2}$ at 28 eV [26]) were observed only in Cr,Ta-TiO_2 as shown in **Figure 2(b)** and **Figure 2(c)**, respectively. In **Figure 2(d)**, the O 1s spectra are shown, however, they contain the spectra originated from the carbon tape. So, we are unable to discuss the valency of O and oxygen defects from these spectra. However, we consider that the prepared TiO_2 and Cr,Ta-TiO_2 do not have much oxygen defects because both of them contain Ti as Ti^{4+} and Cr,Ta-TiO_2 has Cr and Ta as Cr^{3+} and Ta^{5+}.

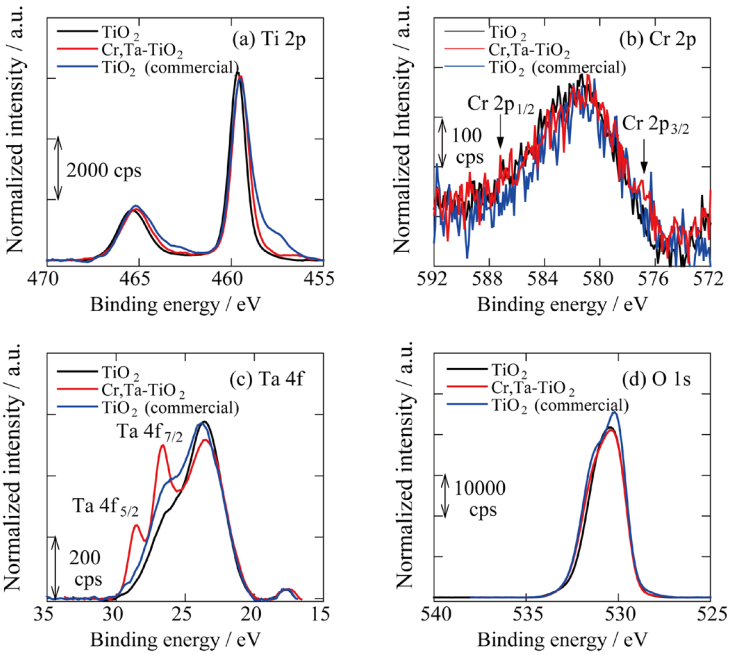

Figure 2. XPS spectra for (a) Ti 2p, (b) Cr 2p, (c) Ta 4f, and (d) O 1s of the prepared TiO_2, Cr,Ta-TiO_2, and commercial TiO_2.

Figures 3(a)-3(d) show the spectra for the Sr 3d, Ti 2p, Rh 3d, and O1s orbitals, respectively, of the prepared $SrTiO_3$, Rh-$SrTiO_3$, and commercially available $SrTiO_3$ (99% purity, Aldrich) after calibration with the C 1s peak similarly. The Sr 3d spectrum peak positions ($Sr3d_{5/2}$ at 132 eV and Sr $3d_{3/2}$ at 134 eV [27]) were quite similar among the prepared $SrTiO_3$, Rh-$SrTiO_3$, and the commercial $SrTiO_3$. However, the spectrum shape of Rh-$SrTiO_3$ was different from those of both types of $SrTiO_3$ (**Figure 3(a)**). According to Ehre *et al*., the Sr 3d spectrum peak positions shift to higher energy region when $SrTiO_3$ becomes amorphous [27]. So, the Sr-O bonding in Rh-$SrTiO_3$ would be looser than that in $SrTiO_3$. As for Ti 2p, Rh-$SrTiO_3$ had shoulders at higher energy side (**Figure 3(b)**), indicating the existence of the structure similar to Ti_3O_5 [28]. So, the oxygen defects were presumably incorporated in Rh-$SrTiO_3$. The Rh3d peaks were observed only in Rh-$SrTiO_3$ as shown in **Figure 3(c)**. In **Figure 3(d)**, the observed O 1s spectra contain those originated from the carbon tape. So, we are unable to discuss the valency of O and oxygen defects from these spectra. However, as mentioned above, Rh-$SrTiO_3$ possibly contains oxygen defects.

The UV-visible absorption spectra of TiO_2, Cr,Ta-TiO_2, Pt/Cr,Ta-TiO_2, $SrTiO_3$, Rh-$SrTiO_3$, and Ru/Rh-$SrTiO_3$ are shown in **Figure 4**. In the spectrum of Cr,Ta-TiO_2, an absorption shoulder in the visible-light region and a negligible shift of the absorption edges were observed compared to that of TiO_2. These findings indicate that the band-gap of Cr,Ta-TiO_2 did not markedly differ from that of TiO_2. In contrast, absorption in the entire range of visible light was observed for Rh-$SrTiO_3$, with a peak occurring at ~600 nm. Konda *et al*. reported the existence of two different doped Rh species as mentioned above is responsible for this spectral pattern [23]. The absorption with a peak occurring at ~600 nm

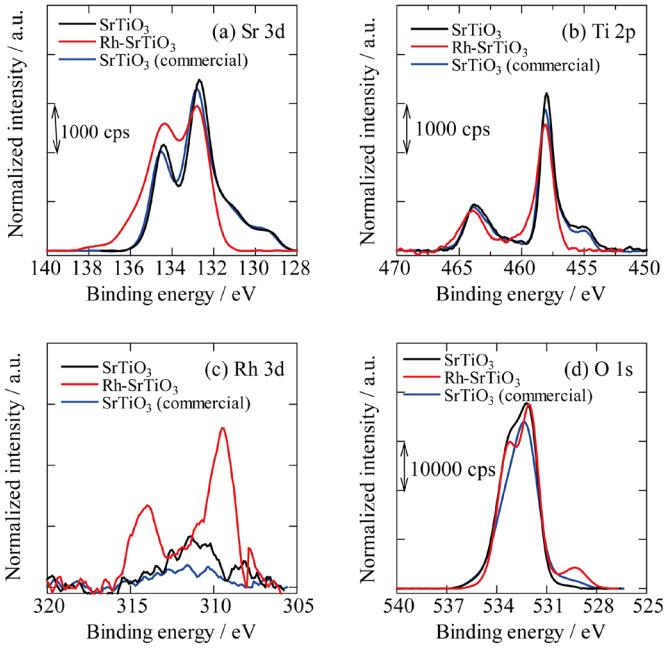

Figure 3. XPS spectra for (a) Sr 3d, (b) Ti 2p, (c) Rh 3d, and (d) O 1s of the prepared $SrTiO_3$, Rh-$SrTiO_3$, and commercial $SrTiO_3$.

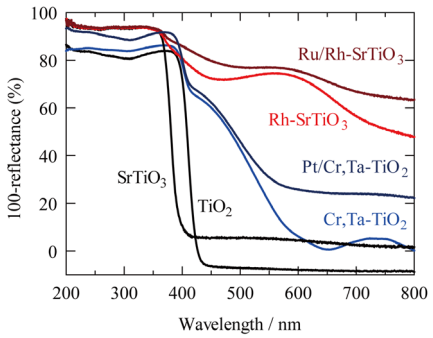

Figure 4. UV-visible absorption spectra of TiO_2, Cr,Ta-TiO_2, Pt/Cr,Ta-TiO_2, $SrTiO_3$, Rh-$SrTiO_3$and Ru/Rh-$SrTiO_3$.

originated from the higher oxidation state of the Rh species, and the one with shorter wavelength region from Rh^{3+}. Also, they asserted that the band-gap of $Sr(Ti_{0.99}Rh_{0.01})O_3$ (*i.e.*, Rh-$SrTiO_3$ in the present study) is narrowed by the partial overlap of Rh $4d^6$ (Rh^{3+}) and O 2p orbitals to form the VB, resulting in a negative-potential shift of the VB top, which we confirmed in our previous study [19]. After depositing either Pt or Ru onto Cr,Ta-TiO_2 or Rh-$SrTiO_3$, respectively, the absorption over a wider wavelength region (>400 nm) clearly increased, indicating the successful deposition of Pt or Ru.

STEM imaging of Pt/Cr,Ta-TiO_2 and Ru/Rh-$SrTiO_3$ are shown in **Figure 5(a)** and **Figure 5(b)**, respectively. The particle sizes of Cr,Ta-TiO_2 and Rh-$SrTiO_3$ were estimated to have sizes of ~100 nm and ~50 nm, respectively. The difference in particle sizes reflected the BET surface areas, which were observed to be 1.4 to 2.8 m^2/g for Cr,Ta-TiO_2 and Rh-$SrTiO_3$, respectively. Both Cr,Ta-TiO_2 and Rh-$SrTiO_3$ particles were connected with each other, *i.e.*, "necking growth" was

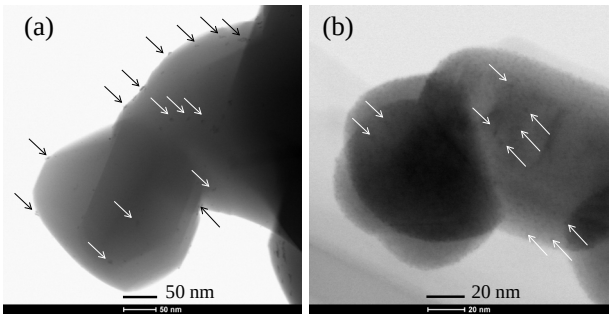

Figure 5. STEM images of Pt/Cr,Ta-TiO_2 (a) and Ru/Rh-$SrTiO_3$ (b). Arrows show cocatalysts, either Pt or Ru.

observed due to rather high calcination temperature and long calcination time (900˚C for 24 h and 1000˚C for 10 h). Nanometer order of Pt on Cr,Ta-TiO_2 and Ru on Rh-$SrTiO_3$ could be observed (indicated by an arrow), and Pt sizes were larger than Ru the reason for which is not clear. From these observations, we also confirmed the deposition of Pt and Ru cocatalysts on Cr,Ta-TiO_2 and Rh-$SrTiO_3$, respectively.

3.2. Half Reactions of Water-Splitting

We examined the evolution of H_2 and O_2 by Ru/Rh-$SrTiO_3$ and Pt/Cr,Ta-TiO_2 in the presence of I^- and IO_3^- as sacrificial agents, respectively, under irradiation with visible light (420-nm LED) as shown in **Figure 6**. H_2 evolution proceeded over Ru/Rh-$SrTiO_3$ in the presence of I^-. According to our previous paper [19], only the negligibly small amount of H_2 was observed over bare Rh-$SrTiO_3$ in the presence of I^-. Thus, we concluded that in the case of Rh-$SrTiO_3$, the cocatalyst Ru on Rh-$SrTiO_3$ was considered as the active site for H_2 evolution. O_2 evolution was detected for Pt/Cr,Ta-TiO_2 (Pt/$Ti_{0.986}Cr_{0.007}Ta_{0.007}O_2$) in the presence of IO_3^-. **Figure 6** also includes the O_2 evolution in the presence of Pt/$Ti_{0.982}Cr_{0.009}Ta_{0.009}O_2$ quoted from our paper [20]. We could enhance the O_2 evolution by changing the amounts of Cr and Ta at Ti. The present Cr,Ta-TiO_2 ($Ti_{0.986}Cr_{0.007}Ta_{0.007}O_2$) is the optimized composition for H_2 evolution for now.

3.3. Two-Step Overall Water Splitting

We next examined water-splitting by the Ru/Rh-$SrTiO_3$ and Pt/Cr,Ta-TiO_2 photocatalysts under visible-light irradiation (420-nm LED) for ~350 h in the presence of IO_3^- ($/I^-$) as a redox mediator (**Figure 7**). As shown in **Figure 7** in the first cycle, H_2 and O_2 evolutions were initially supressed, but then increased. In contrast, in the second and third cycles, such an induction period for H_2 and O_2 evolutions was not observed. Although the reason for the delay in the evolutions was unclear, such phenomenon is frequently encountered. It may be due to the surface restructuring of the photocatalysts and/or cocatalysts, or due to the consumptions of holes and electrons for the residual contaminants on the surfaces of the photocatalysts and remaining oxygen in aqueous solution, respectively. In the third cycle, water-splitting activity decreased likely due to the

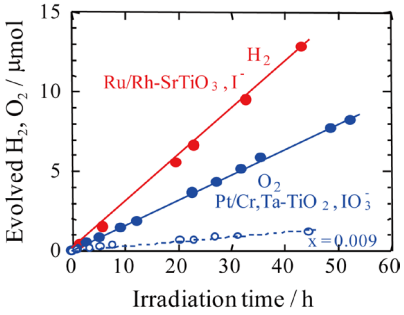

Figure 6. Time courses of H_2 and O_2 evolution resulting from the half reaction of waterbyRu/Rh-$SrTiO_3$ and Pt/Cr,Ta-TiO_2 photocatalysts irradiated with visible light (420-nm LED) in the presence of I^- and IO_3^-, respectively. O_2 evolution was also included over $Pt/Ti_{0.982}Cr_{0.009}Ta_{0.009}O_2$ irradiated with 420-nm LED light in the presence of IO_3^-. The data were replotted from ref. [20].

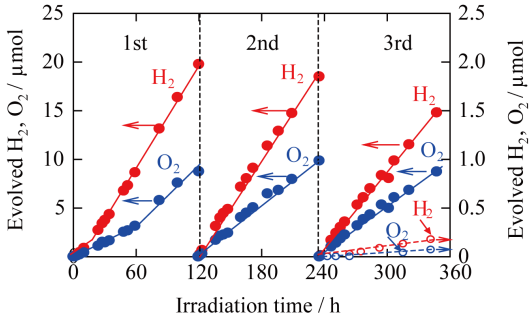

Figure 7. Time courses of H_2 and O_2 evolution resulting from photocatalytic overall water-splitting by Ru/Rh-$SrTiO_3$ and Pt/Cr,Ta-TiO_2 photocatalysts under irradiation with visible light (420-nm LED). The reaction was allowed to proceed for ~350 h with twice evacuations of the system. Those by $Pt/Ti_{0.96}Cr_{0.02}Ta_{0.02}O_2$ and $Pt/Ti_{0.982}Cr_{0.009}Ta_{0.009}O_2$ under 420-nm LED light were also included in the 3rd cycle. The data were replotted from ref. [20].

detachment of cocatalysts. In addition, the amount of water decreased and the partial sample powders attached to the inner wall of the reaction vessel as the repeating cycle increased. These are possible reasons for the decrement in the water-splitting activity in the third cycle. However, H_2 to O_2 were evolved in nearly stoichio-metric (~2 to 1) amounts during each irradiation cycle.

It is well-known that the electron-and-hole transfers between the redox mediators needed for the two-step system and two types of photocatalysts are not efficient. In addition, the redox mediators usually give undesirable effects, e.g., backward reactions to form water from evolved H_2 and O_2. However, the H_2 and O_2 generation rates form the overall water-splitting reaction (0.17 and 0.09 μmol h^{-1}, respectively, in the second cycle) were more than one-half of those from the half reaction of water-splitting (0.29 and 0.16 μmol·h^{-1} for H_2 and O_2 rates, respectively, in **Figure 6**). To our knowledge, the efficiency of H_2 and O_2 generations from the overall water-splitting is rather high. The reason is still unclear; however an affinity between photocatalysts and the redox mediators in the constructed system would be suitable because it actually limits those combinations

to several systems [13].

As determined by XRF analysis, the Ru/Rh-$SrTiO_3$ sample contained Ru at a molar percentage of 1×10^{-2} (1 mol%). Therefore, because a total of 10 mg of Ru/Rh-$SrTiO_3$ was used in the water-splitting experiment as the H_2-photocatalyst, the amount of Ru was 5×10^{-1} μmol. As the total amount of H_2 generated during the 350-h experiment was 53 μmol, we estimated that the turnover number, the ratio of total amount of produced to H_2 to that of Ru co-catalyst, was ~100, which exceeded 1, indicating that this reaction proceeded catalytically. These results demonstrate that the photocatalytic overall water-splitting was achieved in this system. The possible mechanism for the overall water splitting by Pt/Cr,Ta-TiO_2 and Ru/Rh-$SrTiO_3$ is schematically illustrated in **Figure 8**. Visible light-excited electrons in the conduction band of Rh-$SrTiO_3$ are thought to reduce H_2O and generate H_2 and holes in the valence band of Cr,Ta-TiO_2 oxidize H_2O and produce O_2. In contrast, visible-light-excited holes in the VB of Rh-$SrTiO_3$ and electrons in the isolated Cr 3d state contribute to the turnover of I^- to IO_3^-, respectively, and vice versa [19] [20].

When we compare our previous system ($Pt/Ti_{0.96}Cr_{0.02}Ta_{0.02}O_2$ and $Pt/Ti_{0.982}Cr_{0.009}Ta_{0.009}O_2$ [20]) as indicated in the third cycle in **Figure 7**, the H_2 and O_2 generation rates acheved ~100 times higher in the present system, constructed by Ru/Rh-$SrTiO_3$ and Pt/Cr,Ta-TiO_2. It is plausible that the composition of Cr,Ta-TiO_2 ($Ti_{0.986}Cr_{0.007}Ta_{0.007}O_2$) was optimized as the O_2- photocatalyst and that the effective Ru/Rh-$SrTiO_3$ was utilized as the H_2- photocatalyst. In addition, the commercial P-25 TiO_2 (Degussa) and famous nitrogen-doped TiO_2 could evolve only a trace amount of H_2 under the identical 420-nm LED (data not shown) and could not achieve the overall water-splitting. So the present system would be one of the candidates for obtaining H_2 as it consists of environmental-friendly elements.

4. Conclusions

We established a two-step overall water-splitting system that is sensitive to visible light by utilizing TiO_2-based and $SrTiO_3$-based photocatalysts that simulta-

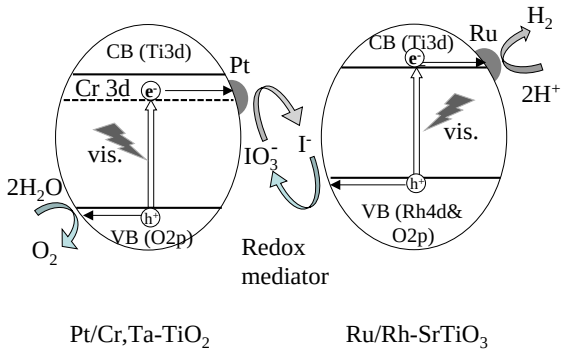

Figure 8. Schematic illustrations of spontaneous H_2 and O_2 evolution by Pt/Cr,Ta-TiO_2 and Ru/Rh-$SrTiO_3$ under irradiation with visible light in the presence of IO_3^-/I^- redox mediator.

neously evolve H_2 and O_2 at a molar ratio of ~2 to 1 efficiently in the presence of IO_3^- ($/I^-$). However, it is necessary to further enhance the visible light sensitivity. This will require the preparation of these TiO_2- and $SrTiO_3$-based photocatalysts which are deficient-free, more highly crystallized, and smaller-sized particles. As is known, TiO_2-based photocatalysts are attractive. So, we are now optimizing the types of dopants and concentrations to further enhance the visible-light sensitivity of TiO_2-based photocatalysts. Moreover, we have recently developed a solid-state two-step overall water-splitting photocatalyst, in which the H_2- and O_2-evolution photocatalysts were connected via silver. In this system, distilled water could be split without a redox mediator. The construction of solid-state systems using TiO_2-based and $SrTiO_3$-based photocatalysts in the present study may be advantageous for industrial and practical applications, as no chemicals are required as redox mediators.

References

[1] Fujishima, A. and Honda, K. (1972) Electrochemical Photolysis of Water at a Semiconductor Electrode. *Nature*, **238**, 37-38. https://doi.org/10.1038/238037a0

[2] Kato, H., Asakusa, K. and Kudo, A. (2003) Highly Efficient Water Splitting into H_2 and O_2 over Lanthanum-Doped $NaTaO_3$ Photocatalysts with High Crystallinity and Surface Nanostructure. *Journal of the American Chemical Society*, **125**, 3082-3089. https://doi.org/10.1021/ja027751g

[3] Maeda, K., Teramura, K., Lu, D., Takata, T., Saito, N., Inoue, Y. and Domen, K. (2006) Photocatalyst Releasing Hydrogen from Water. *Nature*, **440**, 295. https://doi.org/10.1038/440295a

[4] Yoneyama, H., Koizumi, M. and Tamura, H. (1979) Photolysis of Water on Illuminated Strontium Titanium Trioxide. *Bulletin of the Chemical Society of Japan*, **52**, 3449-3450. https://doi.org/10.1246/bcsj.52.3449

[5] Kato, H. and Kudo, A. (2002) Visible-Light-Response and Photocatalytic Activities of TiO_2 and $SrTiO_3$ Photocatalysts Codoped with Antimony and Chromium. *The Journal of Physical Chemistry B*, **106**, 5029-5034. https://doi.org/10.1021/jp0255482

[6] Niishiro, R., Konta, R., Kato, H., Chun, W.J., Asakura, K. and Kudo, A. (2007) Photocatalytic O_2 Evolution of Rhodium and Antimony-Codoped Rutile-Type TiO_2 under Visible Light Irradiation. *Journal of Physical Chemistry C*, **111**, 17420-17426. https://doi.org/10.1021/jp074707k

[7] Li, L., Yan, J., Wang, T., Zhao, Z.J., Zhang, J., Gong, J. and Guan, N. (2015) Sub-10 nm Rutile Titanium Dioxide Nanoparticles for Efficient Visible-Light-Driven Photocatalytic Hydrogen Production. *Nature Communications*, **6**, 5881/1-5881/10.

[8] Maeda, K., Takata, T., Hara, M., Saito, N., Inoue, Y., Kobayashi, H. and Domen, K. (2005) GaN:ZnO Solid Solution as a Photocatalyst for Visible-Light-Driven Overall Water Splitting. *Journal of the American Chemical Society*, **127**, 8286-8287. https://doi.org/10.1021/ja0518777

[9] Sayama, K., Mukasa, K., Abe, R., Abe, Y. and Arakjawa, H. (2002) A New Photocatalytic Water Splitting System under Visible Light Irradiation Mimicking a Z-Scheme Mechanism in Photosynthesis. *Journal of Photochemistry and Photobiology A*: *Chemistry*, **148**, 71-77. https://doi.org/10.1016/S1010-6030(02)00070-9

[10] Kato, H., Sasaki, Y., Iwase, A. and Kudo, A. (2007)Role of Iron Ion Mediator on Photocatalytic Overall Water Splitting under Visible Light Irradiation Using Z-Scheme Systems. *Bulletin of the Chemical Society of Japan*, **80**, 2457-2464.

https://doi.org/10.1246/bcsj.80.2457

[11] Kudo, A. (2007) Recent Progress in the Development of Visible Light Driven Powdered Photocatalysts for Water Splitting. *International Journal of Hydrogen Energy*, **32**, 2673-2678. https://doi.org/10.1016/j.ijhydene.2006.09.010

[12] Maeda, K., Abe, R. and Domen, K. (2011) Role and Function of Ruthenium Species as Promoters with TaON-Based Photocatalysts for Oxygen Evolution in Two-Step Water Splitting under Visible Light. *Journal of Physical Chemistry Letters*, **115**, 3057-3064. https://doi.org/10.1021/jp110025x

[13] Sasaki, Y., Nemoto, H., Saito, K. and Kudo, A. (2009) Solar Water Splitting Using Powdered Photocatalysts Driven by Z-Schematic Interparticle Electron Transfer without an Electron Mediator. *Journal of Physical Chemistry C*, **113**, 17536-17542. https://doi.org/10.1021/jp907128k

[14] Iwase, A., Ng, Y.H., Ishiguro, Y., Kudo, A. and Amal, R. (2011) Reduced Graphene Oxide as a Solid-State Electron Mediator in Z-Scheme Photocatalytic Water Splitting under Visible Light. *Journal of the American Chemical Society*, **133**, 11054-11057. https://doi.org/10.1021/ja203296z

[15] Jia, Q., Iwase, A. and Kudo, A. (2014) $BiVO_4$-Ru/$SrTiO_3$: Rh Composite Z-Scheme Photocatalyst for Solar Water Splitting. *Chemical Science*, **5**, 1513-1519. https://doi.org/10.1039/c3sc52810c

[16] Kobayashi, R., Tanigawa, S., Takashima, T., Ohtani, B. and Irie, H. (2014) Silver-Inserted Heterojunction Photocatalysts for Z-Scheme Overall Pure-Water Splitting under Visible-Light Irradiation. *Journal of Physical Chemistry C*, **118**, 22450-22456. https://doi.org/10.1021/jp5069973

[17] Kobayashi, R., Kurihara, K., Takashima, T., Ohtani, B. and Irie, H. (2016) A Silver-Inserted Zinc Rhodium Oxide and Bismuth Vanadium Oxide Heterojunction Photocatalyst for Overall Pure-Water Splitting under Red Light. *Journal of Materials Chemistry A*, **4**, 3061-3067. https://doi.org/10.1039/C5TA08468G

[18] Kobayashi, R., Takashima, T., Tanigawa, S., Takeuchi, S., Ohtani, B. and Irie, H. (2016) A Heterojunction Photocatalyst Composed of Zinc Rhodium Oxide, Single Crystal-Derived Bismuth Vanadium Oxide, and Silver for Overall Pure-Water Splitting under Visible Light up to 740 nm. *Physical Chemistry Chemical Physics*, **18**, 27754-27760. https://doi.org/10.1039/C6CP02903E

[19] Hara, S., Yoshimizu, M., Tanigawa, S., Ni, L., Ohtani, B. and Irie, H. (2012) Hydrogen and Oxygen Evolution Photocatalysts Synthesized from Strontium Titanate by Controlled Doping and Their Performance in Two-Step Overall Water Splitting under Visible Light. *Journal of Physical Chemistry C*, **116**, 17458-17463. https://doi.org/10.1021/jp306315r

[20] Tanigawa, S. and Irie, H. (2016) Visible-Light-Sensitive Two-Step Overall Water-Splitting Based on Band Structure Control of Titanium Dioxide. *Applied Catalysis B*: *Environmental*, **180**, 1-5. https://doi.org/10.1016/j.apcatb.2015.06.008

[21] Lei, N., Tanabe, M. and Irie, H. (2013) Visible-Light Induced Overall Water-Splitting Photocatalyst: Conduction Band-Controlled Silver Tantalate. *Chemical Communications*, **49**, 10094-10096. https://doi.org/10.1039/c3cc45222k

[22] Shannon, R.D. and Prewitt, C.T. (1969) Effective Ionic Radii on Oxides and Fluorides. *Acta Crystallographica Section B*, **25**, 925-946. https://doi.org/10.1107/S0567740869003220

[23] Konda, R., Ishii, T., Kato, H. and Kudo, A. (2004) Photocatalytic Activities of Noble Metal Ion Doped $SrTiO_3$ under Visible Light Irradiation. *Journal of Physical Chemistry B*, **108**, 8992-8995. https://doi.org/10.1021/jp049556p

[24] Inturi, S.N.R., Boningari, T., Suidan, M. and Smirniotis, P.G. (2014) Flame Aerosol Synthesized Cr Incorporated TiO_2 for Visible Light Photodegradation of Gas Phase Acetonitrile. *Journal of Physical Chemistry C*, **118**, 231-242. https://doi.org/10.1021/jp404290g

[25] Gönüllü, Y., Haidry, A.A. and Saruhan, B. (2015) Nanotubular Cr-Doped TiO_2 for Use as High-Temperature NO_2 Gassensor. *Sensors & Actuators, B*: *Chemical*, **217**, 78-87. https://doi.org/10.1016/j.snb.2014.11.065

[26] Obata, K., Hiroshi, I. and Hashimoto, K. (2007) Enhanced Photocatalytic Activities of Ta, N Co-Doped TiO_2 Thin Films under Visible Light. *Sensors & Actuators, B*: *Chemical*, **339**, 124-132. https://doi.org/10.1016/j.chemphys.2007.07.044

[27] Ehre, D., Cohen, H., Lyahovitskaya, V. and Lubomirsky, I. (2008) X-Ray Photoelectron Spectroscopy of Amorphous and Quasiamorphous Phases of $BaTiO_3$ and $SrTiO_3$. *Physical Review B*, **77**, Article ID: 184106. https://doi.org/10.1103/PhysRevB.77.184106

[28] Moulder, J.F., Stickle, W.F., Sobol, P.E., Bomben, K.D., Chastain, L. and King Jr., R.C. (1995) Handbook of X-Ray Photoelectron Spectroscopy. Physical Electronics Inc., Chanhassen.